AGU PUBLICATIONS

Tectonics

RESEARCH ARTICLE
10.1002/2013TC003450

Key Points:
- Glacially induced faults were critically stressed before glaciation
- Steep-dipping faults can be activated with a low friction value in the crust
- Low-dipping glacially induced faults may slip up to 63 m

Supporting Information:
- Readme
- Tables S1–S3

Correspondence to:
R. Steffen,
rebekka.steffen@geo.uu.se

Citation:
Steffen, R., H. Steffen, P. Wu, and D. W. Eaton (2014), Stress and fault parameters affecting fault slip magnitude and activation time during a glacial cycle, *Tectonics*, *33*, 1461–1476, doi:10.1002/2013TC003450.

Received 30 SEP 2013
Accepted 11 JUL 2014
Accepted article online 17 JUL 2014
Published online 31 JUL 2014

Stress and fault parameters affecting fault slip magnitude and activation time during a glacial cycle

Rebekka Steffen[1,2], Holger Steffen[1,3], Patrick Wu[1,4], and David W. Eaton[1]

[1]Department of Geoscience, University of Calgary, Calgary, Alberta, Canada, [2]Department of Earth Sciences, Uppsala University, Uppsala, Sweden, [3]Lantmäteriet, Gävle, Sweden, [4]Department of Earth Sciences, University of Hong Kong, Hong Kong

Abstract The growing and melting of continental ice sheets during a glacial cycle is accompanied by stress changes and reactivation of faults. To better understand the relationship between stress changes, fault activation time, fault parameters, and fault slip magnitude, a new physics-based two-dimensional numerical model is used. In this study, tectonic background stress magnitudes and fault parameters are tested as well as the angle of the fault and the fault locations relative to the ice sheet. Our results show that fault slip magnitude for all faults is mainly affected by the coefficient of friction within the crust and along the fault and also by the depth of the fault tip and angle of the fault. Within a compressional stress regime, we find that steeply dipping faults (~75°) can be activated after glacial unloading, and fault activity continues thereafter. Furthermore, our results indicate that low-angle faults (dipping at 30°) may slip up to 63 m, equivalent to an earthquake with a minimum moment magnitude of 7.0. Finally, our results imply that the crust beneath formerly glaciated regions was close to a critically stressed state, in order to enable activation of faults by small changes in stress during a glacial cycle.

1. Introduction

The stress state along a fault affects its stability, and if it is changed, faults that were formerly inactive can be reactivated. Several factors, such as change in pore fluid pressure, may alter stress condition. Additionally, changes in the stress field can be induced by the glacial isostatic adjustment (GIA) process. GIA includes all processes related to uplift and subsidence of the crust induced by surface loading and unloading of an ice sheet. Crust and mantle are affected by GIA, and the observations of GIA (e.g., relative sea level, land-uplift rate by GPS, and gravity data) below formerly and currently glaciated regions are used to infer the viscosity of the mantle and thickness of lithosphere, which is the outer layer of the Earth with an elastic rheology (see *Steffen and Wu* [2011] for a summary).

During glaciation, the weight of the ice sheet generates a vertical stress in the lithosphere, but the flexure of the lithosphere induces horizontal bending stresses as well, which change all components of the stress tensor [e.g., *Johnston*, 1987]. Depending on the size of the ice sheet, the vertical stress can be either larger or smaller than the horizontal stress [e.g., *Johnston et al.*, 1998]. During deglaciation, the ice sheet melts and the vertical stress decreases. However, the horizontal stress in the lithosphere decreases much more slowly due to the viscoelastic properties of the lithosphere and the associated upward migration of stress as the mantle relaxes. At the end of deglaciation, vertical stresses due to GIA and the ice sheet vanish, but the horizontal stresses still exist, thus affecting fault stability in deglaciated regions such as Europe and North America. In both regions, faults reactivated during and after the end of deglaciation at the last Ice Age have been identified due to visible fault offsets of glacially abraded rocks [e.g., *Kujansuu*, 1964; *Lagerbäck*, 1978; *Olesen*, 1988; *Muir-Wood*, 1993] or Pleistocene unconsolidated sediments [*Brandes et al.*, 2012]. Moreover, fault offsets and activation times were also inferred from relative sea level data and dating of mudslumping events [e.g., *Dyke et al.*, 1991; *Shilts et al.*, 1992; *Fenton*, 1994]. These faults are called glacially induced faults (GIFs).

In North America, estimated GIF offsets vary between a few decimeters and 100 m [e.g., *Dyke et al.*, 1991; *Fenton*, 1994], of which the latter is located in the Canadian Arctic and is the largest inferred GIF offset [*Dyke et al.*, 1991]. In Fennoscandia, fault offsets of up to 30 m are found and are mostly located in the Lapland Province (northern Sweden/Finland/Norway [e.g., *Kujansuu*, 1964; *Lagerbäck*, 1978; *Olesen*, 1988;

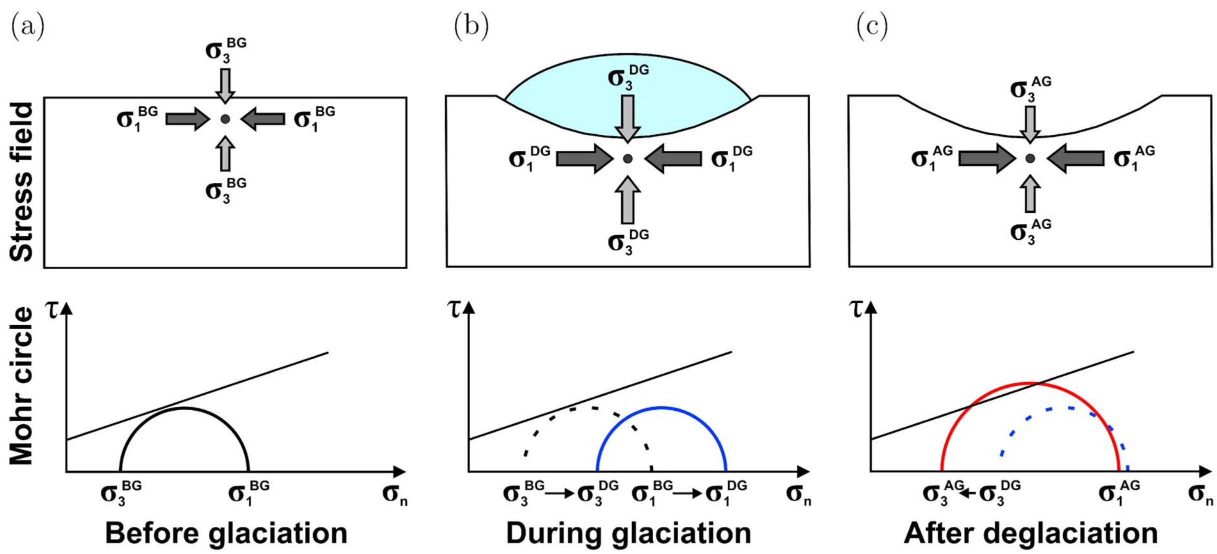

Figure 1. Sketch of fault stability (a) before, (b) during, and (c) after glaciation for a thrusting background stress regime. The top row refers to the stress field condition at a point in the crust, and the bottom row indicates the maximum and minimum principal stresses σ_1 and σ_3 in a Mohr diagram. The black half circle presents the stress condition before glaciation, the blue half circle during glaciation, and the red half circle after glaciation. The dotted line is used to indicate the stress condition at the time point before. The straight line in all Mohr diagrams represents the line of failure.

Muir-Wood, 1993; *Munier and Fenton*, 2004]). In addition to GIFs in northern Sweden, indications for these faults are also found in northern Germany and southern and central Sweden [*Brandes et al.*, 2012; *Jakobsson et al.*, 2014; *Smith et al.*, 2014]. It is assumed that these faults are reactivated complex fault zones. The only seismic profile crossing a GIF in northern Sweden indicated a steep dip angle of more than 50° [*Juhlin et al.*, 2009]. Although, in general, these faults have been reactivated with a reverse sense of movement consistent with compressional stress conditions [e.g., *Adams*, 1989; *Mazotti and Townend*, 2010; *Steffen and Wu*, 2011; *Steffen et al.*, 2012], in some deglaciated areas normal or strike-slip regimes exist [e.g., *Stein et al.*, 1979, 1989; *Quinlan*, 1984; *Slunga*, 1991; *Zoback*, 1992; *Muir-Wood*, 1993; *Arvidsson*, 1996; *Lund and Zoback*, 1999].

Fennoscandia and North America are not only known for the existence of GIFs but also for stable cratonic settings [e.g., *Hoffman*, 1989; *Kinck et al.*, 1993]. Consequently, earthquakes with large magnitudes are generally not expected in these areas. Furthermore, as the tectonic stress, resulting from constant plate boundary forces (ridge push within both areas), is assumed to be effectively constant during a glacial cycle of about 100 ka [*Luttrell and Sandwell*, 2010], the observed increase in seismicity close to the end of deglaciation implies that these events are associated with GIA.

In order to analyze the behavior of GIFs, a thrusting background stress state is assumed in correspondence to the observed stress settings in formerly glaciated regions. A thrusting regime is characterized by maximum and intermediate principal stresses that lie close to the horizontal direction and a near-vertical minimum principal stress. By applying the general Anderson-Coulomb theory, the effects of a thrusting stress regime in combination with GIA stresses can be explained using a Mohr diagram (see Figure 1). It was shown by *Célérier* [1988, 1995] that the Anderson-Coulomb theory works well for the analysis of reactivated faults. During glacial loading, the additional vertical and horizontal stresses increase all three principal stresses, and the Mohr circle moves in the positive direction along the normal stress (σ_n). This moves the Mohr circle away from the line of failure, as the change in the radius of the circle is less than the net displacement of the Mohr circle (Figure 1b); hence, fault movement is suppressed. As soon as the ice melts, the vertical load decreases, but the flexure in the lithosphere responds more slowly. The radius of the Mohr circle thus increases, and the midpoint of the circle moves back toward the shear stress (τ) axis (Figure 1c). If the Mohr circle touches or crosses the line of failure, the fault will slip, releasing stress in the form of earthquakes.

Thus, GIA-induced stress can trigger fault slips for optimally orientated faults. However, the observed GIFs are steeply dipping and not optimally orientated, whereas thrust faults are normally associated with gently

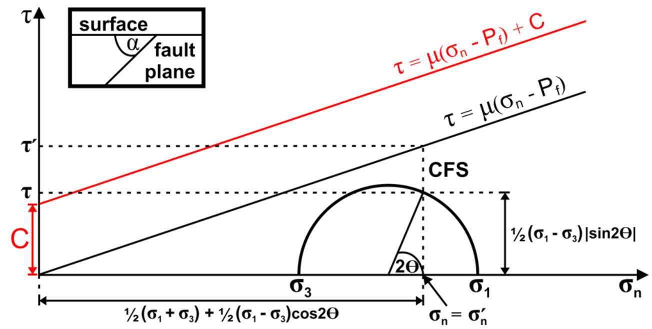

Figure 2. Fault stability *CFS* defined as the difference in shear stress between the Mohr circle and the line of failure (without cohesion *C*, black line).

dipping faults only and it is questionable whether high-angle reverse faults are compatible with the theory of Anderson-Coulomb [*Suppe*, 1985]. These considerations lead to several questions: Can GIA cause faults to slip along steeply dipping faults? If so, what type of fault parameters are required to activate steeply dipping faults?

Earthquake hazard due to GIA does not only affect formerly glaciated areas but also currently glaciated regions that are undergoing rapid ice melting, e.g., Greenland and Alaska [e.g., *Sauber and Molnia*, 2004; *Larsen et al.*, 2006; *Voss et al.*, 2007; *Dahl-Jensen et al.*, 2010]. Stress changes induced in these regions can generate earthquakes if the background regime favors the additional stresses [e.g., *Wu and Hasegawa*, 1996a]. Therefore, it is important to understand more about stress conditions and fault parameters in these regions.

In this study, we present the results of a new physics-based numerical 2-D model, which is loaded with an ice sheet. Several parameters are tested to evaluate parameter sensitivity with respect to activation time, magnitude of fault slip, and number of events. The aim of this paper is to answer the following questions:

1. How does the magnitude of background stress affect activation time of GIFs?
2. Is the crust before glaciation critically stressed?
3. Can steeply dipping faults be activated in a thrusting background regime with stress changes induced by GIA?
4. What fault parameters are required to cause thrusting along steeply dipping faults?

The stability of the fault and the state of stress are required to carry out this analysis and will be explained in the following section. Afterward, the model setup is summarized, which is followed by a detailed list of results and the respective discussions. The key results are summarized within the conclusion, where the questions raised above are answered.

2. Fault Stability and State of Stress

The analysis of the stability of a fault during a glacial cycle must take into account the background stresses, which can be assumed to be constant during the cycle, and the changes in the GIA stress. The commonly used Coulomb failure stress (CFS) is used to evaluate fault stability in an isotropic crust [see *Ivins et al.*, 1990, Figure 1], and it is defined as follows [*Harris*, 1998; *Steffen et al.*, 2014a]:

$$\mathrm{CFS} = \frac{1}{2}\left[(\sigma_1 - \sigma_3)\,|\sin 2\Theta|\right] - \frac{\mu}{2}\left[(\sigma_1 + \sigma_3) + (\sigma_1 - \sigma_3)\cos 2\Theta\right]. \tag{1}$$

CFS depends on the magnitudes of maximum σ_1 and minimum σ_3 principal stresses, the coefficient of friction μ, and the angle Θ between the maximum principal stress direction and the normal of the fault plane. For simplicity, isotropic material is considered in this study. Pore fluid pressure is neglected as it is insufficiently studied within glacial cycles and is therefore an unknown component. Since the GIA-induced stress is generally not large enough to cause fracture, we consider only the reactivation of preexisting faults by GIA. Now the cohesion of preexisting faults is generally small, so it is assumed to be negligible; moreover, the cohesion parameter is currently not included as a fault property in the ABAQUS software used for the modeling. Positive CFS values indicate instability along the fault, whereas negative values (CFS < 0 MPa) refer to stable conditions (Figure 2).

The background stresses are an important component in the analysis of fault stability and have to be determined separately. The vertical background stress is equal to the overburden pressure and depends on the gravity g, density ρ, and depth z [e.g., *Twiss and Moores*, 2007]:

$$S_V = \int \rho_{\mathrm{layer}}\, g_{\mathrm{layer}}\, \mathrm{d}z. \tag{2}$$

The overburden pressure is also included in the horizontal background stress, but an additional tectonic component has to be taken into account. As preexisting faults are not assumed to be optimally orientated but were close to neutral stability before the onset of glaciation, the horizontal background stress has to depend on the fault angle [*Steffen et al.*, 2014a]. In this preliminary study, we consider only one fault, or equivalently, we assume that other faults that are more optimally oriented are nonexistent or have a very large cohesion. Furthermore, as no other constraints are given for the crust outside of the fault, the same stress conditions have to be assumed. Taking all these assumptions into account, but allowing us to study whether the isotropic crust was critically stressed before deglaciation, a more general expression for the horizontal background stress is used [*Steffen et al.*, 2014a]:

$$S_H = \frac{\beta\left([\mu - \mu\cos 2\Theta + |\sin 2\Theta|]\, S_V + 2\,\mathrm{CFS}^{\mathrm{BG}}\right)}{-[\mu + \mu\cos 2\Theta - |\sin 2\Theta|]} + (1-\beta)\, S_V. \tag{3}$$

The additional parameters β and $\mathrm{CFS}^{\mathrm{BG}}$ are defined to allow greater variation in the magnitude of the background stress in order to investigate whether the crust was critically stressed initially. The β is a scaling factor defining the magnitude of tectonic background stress in the horizontal stress component. If β takes a value of 1, the horizontal stress component consists of maximum tectonic background stress and the crust is critically stressed. However, the tectonic background stress still depends on the vertical stress S_V. In general, a decrease in β promotes greater stability along the fault. The minimum β value is 0, in which case horizontal stress becomes equal to the vertical stress and tectonic stresses are not included. A variation of this parameter enables exploration of the stress conditions before glaciation. As part of our parameter selection process, several values were tested between 0 and 1. However, if a preexisting fault with a certain α and μ is not activated for one β value, lower values were not tested for this fault as a decrease in β relates to a decrease in the magnitude of tectonic background stress and more stable conditions before glaciation. Therefore, β gives the possibility to decrease tectonic background stresses and test if fault reactivation occurs.

$\mathrm{CFS}^{\mathrm{BG}}$ represents the fault stability before glaciation (BG). A negative $\mathrm{CFS}^{\mathrm{BG}}$ increases the distance between line of failure and Mohr circle and therefore leads to more stable conditions. The tectonic background stress decreases in this case, as it can be lowered to reach the state given by the Mohr circle. However, a positive $\mathrm{CFS}^{\mathrm{BG}}$ value assumes movement of the fault before glaciation and therefore increased magnitudes in the tectonic background stress. In former studies, the factor $\mathrm{CFS}^{\mathrm{BG}}$ was set to 0 MPa [e.g., *Wu*, 1996, 1997; *Wu and Hasegawa*, 1996a, 1996b; *Lund*, 2005; *Lund et al.*, 2009].

A third parameter, which is allowed to change, is the coefficient of friction for the tectonic background stress μ_{back}. The parameter varies between 0 and 1 but lies mostly in the range between 0.2 and 0.6. We remark that the coefficient of friction can also be applied as a surface parameter of the fault [*Nüchter and Ellis*, 2010], and we use the symbol μ_{fault} here. Different values can be assumed for both coefficients of friction, and former studies suggest values between 0.4 and 0.6 [*Byerlee*, 1978; *Rivera and Kanamori*, 2002]. However, μ_{back} also influences the angle of the fault that can be (re-)activated in a rock mass, and with a decrease in the friction the range of possible fault angles increases [*Abers*, 2009]. As the dip angle of GIFs is not known except for one case (i.e., more than 50° in *Juhlin et al.* [2009]), the relationship between the coefficient of friction and the dip angle of GIFs is not well known, so we can only make assumptions concerning the coefficient of friction of the crust.

The above mentioned parameters show a wide range of expected values and affect the magnitude of the horizontal stress and the fault itself but have no effect on the GIA model. The aim of this paper is to increase our understanding about these parameters and how they affect fault slip magnitude and activation time during a glacial cycle. An increased knowledge is important to the development of more advanced and realistic models for estimation of the hazard of glacially induced earthquakes. Note that parameters within the GIA model are not changed in this paper, because a sensitivity of these values has already been studied in an accompanying paper [*Steffen et al.*, 2014b]. In that paper, it is demonstrated that the crustal and lithospheric thickness do not affect the magnitude of fault slip whereas the thickness of the ice sheet has no effect on the fault slip magnitude, while the timing of fault reactivation is controlled by the ice sheet width.

3. Model Setup

The GIA-fault model used within this study contains a viscoelastic earth model with an ice load applied on its surface. The earth model is represented by a six-layer finite element mesh (Figure 3). The upper two

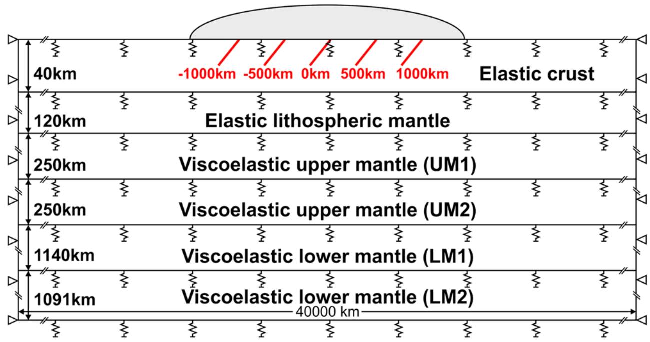

Figure 3. Structure of the model showing location of faults. Springs represent Winkler foundations, and triangles represent the fixed degree of freedom. The ice sheet follows a parabolic shape without any change in the horizontal dimension during a glacial period (grey body on top of the model). Locations of the faults in the crustal layer are presented in red.

layers, which represent the lithosphere, have elastic material parameters (Poisson's ratio, Young's modulus, and density; see Table 1 for values), and the other four layers, which represent the mantle, behave viscoelastically with the viscosity as an additional parameter. The lithosphere has a constant total thickness of 160 km throughout the model.

Lithospheric thickness varies laterally, especially from below the ocean to below the continents, where it can reach 160 km or more below old cratons based on seismological data, e.g., eastern Fennoscandia and below Hudson Bay [e.g., *Kukkonen et al.*, 2003; *Eaton et al.*, 2009; *Eaton and Darbyshire*, 2010; *Darbyshire et al.*, 2013]. However, the thickness of the seismic lithosphere is generally different from that of the mechanical lithosphere, which also depends on the timescale of the loading process [e.g., *Watts and Burov*, 2003]. The results of GIA studies show that the lithosphere below the old craton can be as thick as 160 km [e.g., *Ivins et al.*, 2003; *Steffen and Kaufmann*, 2005; *Steffen et al.*, 2009, 2014c].

The crust, which lies in the upper 40 km of the lithosphere, has a prescribed fault, which is cut into the model and outcrops at the surface, dipping at a prescribed angle. In each model, one fault can be activated during a glacial cycle. The mantle is subdivided into an upper mantle (UM) consisting of two layers and a lower mantle (LM) with two layers as well. The viscosities differ between UM and LM but are constant within each part (Table 1). The model reaches a depth of 2891 km, which is approximately the core-mantle boundary. Material parameters are obtained using the preliminary reference Earth model (PREM) [*Dziewonski and Anderson*, 1981].

The elements in the model are quadrilateral plane strain elements, which have a length of about 700 m in the uppermost 20 km of the model, and reach about 200 km side length at the bottom of the model. Therefore, at least two element layers represent one material layer within the model. These elements assume that no strain occurs in the direction normal to the plane of the model, and stress and strain can vary throughout the element [*Hibbitt et al.*, 2012].

The ice model, which is applied on top of the earth model (Figure 3), represents the first-order changes in ice thickness during the last Ice Age of North America. Based on the finding of *Steffen et al.* [2014b], the size of the ice sheet does not affect the fault slip and throw, only the onset timing. Thus, in this study, the size is chosen to be similar to the Laurentide Ice Sheet. The simplified ice sheet in this study has a width of 3000 km

Table 1. Rheological Parameters and Thickness Given for Each Layer[a]

Layer Name	Thickness (km)	Density (ρ_{layer}) (kg/m^3)	Young's Modulus (GPa)	Poisson's Ratio	Viscosity (Pa s)
Crust	40	3256	157	0.276	-
Lithospheric mantle	120	3370	166	0.286	-
Upper mantle 1 (UM1)	250	3505	197	0.299	$7 \cdot 10^{20}$
Upper mantle 2 (UM2)	250	3908	285	0.296	$7 \cdot 10^{20}$
Lower mantle 1 (LM1)	1140	4798	536	0.285	$20 \cdot 10^{21}$
Lower mantle 2 (LM2)	1091	5341	696	0.301	$20 \cdot 10^{21}$

[a]Density, Young's modulus, and Poisson's ratio are based on preliminary reference Earth model (PREM) [*Dziewonski and Anderson*, 1981]. The viscosity values are obtained from a GIA study in North America using a lithospheric thickness of 160 km [*Steffen et al.*, 2009].

and a thickness of 3500 m and follows a parabolic shape. For simplicity, the ice margin is not allowed to migrate outward during glaciation nor inward during deglaciation. The glacial cycle has a duration of 130 ka consisting of a 100 ka glaciation phase, 10 ka deglaciation phase, and a 20 ka postglacial phase. During the postglacial phase no ice load is applied to the model. A single time step has a duration of 1 ka. Therefore, the accuracy of the activation times is $\pm$500 a. The simplicity of our ice models implies that conclusions drawn from this study might change if multiple ice domes exist, the geometry of the ice follows the coastline, or timing of ice collapsing is complex. Nevertheless, general insights concerning the behavior of fault properties and magnitudes of tectonic background stress can be taken from this pilot study.

The GIA-fault model is similar to other models used in GIA studies but has fault surfaces included, which are allowed to release stresses induced by GIA. As commercial finite element software (e.g., ABAQUS [*Hibbitt et al.*, 2012]) only allow the solution of simple equations of motion and do not include the advection of prestress term, which represents a buoyancy return force and is of primary importance in geoscientific studies, the method has been modified to include a stress transformation [*Wu*, 2004]. This modification implies that the stress output from the finite element model has to be adjusted to give a true estimate of GIA stress. To overcome this and other problems, a new approach has been developed [*Steffen et al.*, 2014a]. This consists of a three-step cascaded model that uses the GIA model as the first model, which computes displacement and stress distributions during a glacial cycle. The results are used in the second and third models, which are created if fault instability exists (CFS $>$ 0). Each finite element in the second and third models contains a stress magnitude determined from the first model including the GIA stress component, and each node is displaced based on the displacement obtained from the first model. Fault slip and the release of GIA stresses in the third model is enabled using an open fault contact and the application of a friction value between opposing fault surfaces. The slip of the fault creates an offset between hanging wall and footwall. A detailed description of this approach can be found in *Steffen et al.* [2014a]. The advantage of this new model [*Steffen et al.*, 2014a] is that the role of GIA-induced stress is explicitly included and not mixed in with the effect of plate motion.

A similar approach was developed by *Hampel and Hetzel* [2006] and numerous thrust-fault results were presented in *Turpeinen et al.* [2008], but their models simplify the effects of GIA stress and neglect the effect of the viscoelastic mantle. However, the mantle is the driving force of the viscoelastic behavior of GIA, and without the mantle, only an elastic GIA effect is taken into account. Furthermore, fault slips in their models are a result of the combined effects of a stress related to GIA and a converging horizontal displacement boundary condition.

4. Results and Discussion

The earth and ice model are not changed within this study, and therefore, the GIA signal is the same for all variations. The magnitude in tectonic background stress depends on the fault angle (see equation (3)) and also on the parameters μ_{back} (coefficient of friction in the crust), CFS^{BG} (fault stability before glaciation), and β (ratio of tectonic background stress in horizontal stress). The angle is varied within all tests as well as the location of the fault.

Four different fault dip angles are tested: 30°, 45°, 60°, and 75°. In addition, the fault location is varied between −1000 km, −500 km, 0 km, 500 km, and 1000 km (Figure 3). All faults are incorporated into the model for all tests; however, only the contact of the specific fault investigated in a test is open, while all other fault contacts are tied and no motion is possible. The variation of the other tectonic background stress parameters is listed in Table 2, with the reference model having a coefficient of friction for the crust (μ_{back}) of 0.4, a fault stability before glaciation (CFS^{BG}) of 0 MPa, which indicates a critically stressed crust, and 100 % tectonic stress in the horizontal stress component ($\beta = 1$). Positive values of CFS^{BG} and values of above 1 for β are not considered as observations indicate that GIFs were probably not active for several million of years and were not active before glaciation started [*Lagerbäck and Sundh*, 2008].

Furthermore, the depth of the fault tip and the coefficient of friction between opposing fault surfaces (μ_{fault}) are varied (Table 2). The fault tip is defined mathematically as the point where both fault surfaces end in the crust and fault movement terminates. The fault tip remains fixed during each test; hence, fault surface growth is not considered. The reference model consists of a fault that extends from the surface to a depth of 8 km and a μ_{fault} of 0.4. Further parameters (cohesion C and pore fluid factor λ) are neglected and set to 0 to decrease the number of potential factors of fault slip and activation time in this study [see *Steffen et al.*, 2014a].

Table 2. Model Parameters and Variations Used in This Study[a]

Model Parameter	Values
Width of ice sheet	**3000 km**
Thickness of ice sheet	**3500 m**
Dipping angle of fault α	30°, **45**°, 60°, 75°
Location of fault (to ice sheet center)	−1000 km, −500 km, **0 km**, 500 km, 1000 km
Coefficient of friction for background stress μ_{back}	0.2, **0.4**, 0.6
Fault stability before glaciation CFS^{BG}	**0 MPa**, −2 MPa, −4 MPa
Tectonic background stress factor β	**1**, 0.95, 0.9
Cohesion C	**0 MPa**
Pore pressure	**0 MPa**
Coefficient of friction along fault μ_{fault}	**0.4**
Depth of fault tip	4 km, **8 km**, 12 km, 16 km

[a]Values of the reference model in bold.

The model estimates fault slip numerically by releasing stresses. The fault slip magnitude is shown over time between 90 ka and 130 ka, as activations before glacial maximum (100 ka) are not predicted by any model for reasons illustrated in Figure 1. The results for different angles and at different locations are plotted; however, the results at locations −500 km and −1000 km are not presented in the figures but can be found in the tables that are part of the supporting information. In general, these results are similar to those found at locations 500 km and 1000 km, respectively.

In the first part of this section, the results of the reference model are discussed to present the main ideas of fault slip magnitudes and activation times and their specific reasons. This is followed by a detailed description of the results and discussion of the sensitivity of each parameter variation.

4.1. Reference Model

Faults in the reference model are activated near the end of deglaciation at 110 ka, and fault slips of more than 10 m are predicted numerically (see Figure 4 and Table S1 in the supporting information). The 30° and 45° faults slip only once, whereas a steeper dipping fault slips for a second time 1–2 ka later. The fault slip during the first event is larger than the second event. In general, the magnitude of fault slip of the first event decreases with an increase in the fault angle (Figure 4).

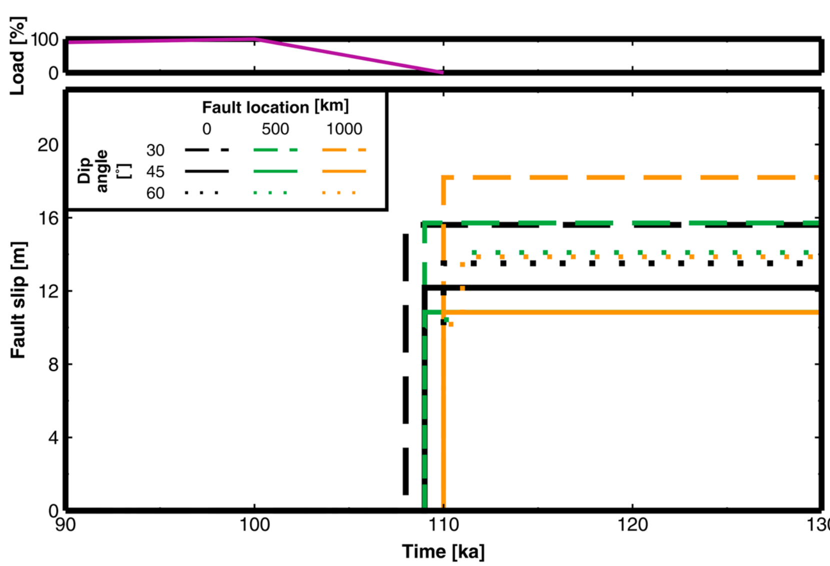

Figure 4. Fault slip for the reference model at different locations (0 km, 500 km, and 1000 km) and fault angles (30°, 45°, and 60°). The time on the x axis refers to the model time running from 0 ka to 130 ka. No fault slip is obtained through the first 100 ka. The purple line in the upper diagram shows the distribution of the ice load during the model time. The following additional parameters were used: μ_{back} of 0.4, μ_{fault} of 0.4, CFS^{BG} of 0 MPa, β of 1, and fault tip depth of 8 km.

Table 3. Stress Magnitudes Depending on Fault Angle and Coefficient of Friction[a]

Fault Angle α	μ_{back}	S_H (MPa)	S_V (MPa)	τ (MPa)	σ_n (MPa)
30°	0.2	244	160	36	181
45°	0.2	240	160	40	200
60°	0.2	273	160	49	245
75°	0.2	666	160	127	632
30°	0.4	353	160	84	208
45°	0.4	374	160	107	267
60°	0.4	642	160	209	522
30°	0.6	500	160	147	245
45°	0.6	641	160	241	401

[a]Horizontal (S_H) and vertical (S_V) background stresses as well as normal (σ_n) and shear (τ) stresses for different fault angles α and coefficient of internal frictions of the crust μ_{back} at a depth of 5 km.

The amount of fault slip is affected by the normal and shear stresses along the fault, which depend on the fault angle and the relationship between maximum and minimum principal stresses σ_1 and σ_3, respectively. The shear stress acts parallel to the fault and causes the sliding of the fault, whereas the normal stress acts perpendicular to the fault surfaces, pressing the surfaces together and preventing fault movement. As σ_3 is the vertical stress in a thrusting regime, it is mainly determined by the overburden pressure and the weight of the ice sheet. Commencing at the start of deglaciation, σ_3 begins to decrease. After the load is completely gone (at 110 ka), the vertical stress is the same as before glaciation, and only overburden pressure is present. The σ_1 is the horizontal stress and is affected by the background stress and the flexure of the lithosphere induced by GIA. The latter starts to decrease at the start of deglaciation, but the rate of decrease is much slower than that of σ_3. Therefore, after the end of deglaciation, only horizontal rebound stress remains in addition to the tectonic background stress. The rebound stresses depend only on the ice and earth model [*Steffen et al.*, 2014b], are independent of the fault angle, and are not changed within this study.

However, the horizontal background stresses required to keep the fault at frictional equilibrium depends on the angles of the fault (see equation (3)). This is shown in Table 3. A 60°-dipping fault implies higher horizontal background stresses in order to be close to initial frictional equilibrium (about 4 times the vertical stress for a coefficient of friction of 0.4; see equation (3)) than 30° and 45° faults with only about 2.2 times and 2.3 times the vertical stress, respectively. However, the fault slip magnitude decreases with an increase in fault angle and an accompanying increase in tectonic background stress (Table 3).

The change in the magnitudes of normal and shear stresses on the fault as a consequence of the stress state in the crust is related to the principal stresses and the fault angle ($\alpha = 90° - \Theta$) by

$$\tau = 0.5\left(\sigma_1 - \sigma_3\right)|\sin 2\Theta|, \tag{4a}$$
$$\sigma_n = 0.5\left(\sigma_1 + \sigma_3\right) + 0.5\left(\sigma_1 - \sigma_3\right)\cos 2\Theta. \tag{4b}$$

This leads to the following equations for each fault angle used in this study:

$$\begin{aligned}
\alpha = 30°: \quad & \tau = 0.433\left(\sigma_1 - \sigma_3\right),\\
& \sigma_n = 0.25\,\sigma_1 + 0.75\,\sigma_3,\\
\alpha = 45°: \quad & \tau = 0.5\left(\sigma_1 - \sigma_3\right),\\
& \sigma_n = 0.5\,\sigma_1 + 0.5\,\sigma_3,\\
\alpha = 60°: \quad & \tau = 0.433\left(\sigma_1 - \sigma_3\right),\\
& \sigma_n = 0.75\,\sigma_1 + 0.25\,\sigma_3,\\
\alpha = 75°: \quad & \tau = 0.25\left(\sigma_1 - \sigma_3\right),\\
& \sigma_n = 0.933\,\sigma_1 + 0.067\,\sigma_3.
\end{aligned}$$

The equations above show that with an increase in the fault angle, the normal stress, which opposes fault movement, has an increasing contribution from the horizontal stress. For the shear stress, which drives the fault slip, the coefficient in front of the stress difference ($\sigma_1 - \sigma_3$) reaches maximum at 45°, but because the stress difference increases with α (see Table 3), the value of shear also increases with steeper dipping fault angle, but its value is always less than that of the normal stress. As a consequence, a steeper dipping fault angle means a smaller fault slip in one event. The length of the fault also increases with a decrease in the angle as the modeled faults are constrained to extend between depth of fault tip and the Earth's surface. A 30° dipping fault is 16 km long, whereas a 60° fault has a length of only 9.24 km. A longer fault slips more and produces larger fault throws [e.g., *Kim and Sanderson*, 2005].

Differences in the fault slip between different locations are related to their specific position of the fault with respect to the ice sheet center. All faults dip in the same direction (see Figure 3), which results in a dip toward the ice sheet center for faults at +500 km and +1000 km (on the positive/right side of the model), and a dip away from the center at −500 km and −1000 km (on the negative/left side of the model). As rebound stresses increase toward the ice sheet center, faults closer to the center slip more. Furthermore, faults on the positive side of the model have more ice applied on the hanging wall, and if the fault is activated during the deglaciation phase, the fault slips less than faults on the negative side of the model. These faults have less ice applied on the hanging wall. However, as soon as deglaciation ends and no ice load is applied on the hanging wall or footwall, the rebound stress plays a more important role, and faults with their tips closer to the center slip more than faults farther away.

In summary, the differences in fault throw for different fault angles and locations can be explained by normal and shear stress directions and magnitudes. The location of a fault with respect to the ice center results in different amounts of ice loading between the hanging wall and the footwall, which determine whether the fault slips more during or after deglaciation.

4.2. Influence of Friction of the Crust μ_{back}

In this subsection, the coefficient of friction (μ_{fault}) at the fault surface remains constant at 0.4, but three values of μ_{back} (0.2, 0.4, and 0.6) are considered. An increase in the coefficient of friction for the crust (μ_{back}) is accompanied by an increase in the horizontal background stress magnitude for the same angles (Table 3) but a decrease in the ratio between normal and shear stress from 5 to 2.5 and 1.7 for an angle of 45°. Therefore, increasing μ_{back} correlates with an increase in fault slip (Figures 5a and 5b; see Table S2 in the supporting information). Steeply dipping faults (60° and 75°) are not activated for a μ_{back} of 0.6. However, reduced μ_{back} of 0.2 allows the activation of 75° faults for the first time and can be compared to results of lower fault angles (Figure 5b). Figures 5a and 5b also show that for μ_{back} of 0.2, an earlier activation is predicted; this also results from lower background stresses and a smaller normal stress.

The GIA stress is not changed; only tectonic background stress changes affect activation time and magnitude of fault slip, and a low value of μ_{back} of 0.2 increases the ratio of GIA stresses to tectonic background stresses since the tectonic background stresses are smaller but GIA stresses are constant. Therefore, a small change in GIA stress has a larger effect in lower background stress magnitudes, and the faults are activated earlier. For larger values of μ_{back}, the vertical loading stress has to be reduced further in order to promote fault instability.

The location of the fault relative to the ice sheet center shows the same behavior as for a fault at the center (Figure 5a). The increase in offset is smaller due to smaller rebound stresses as the location moves farther from the ice center.

The 60° dipping fault (Figure 5b) shows different behaviors for different background stress frictions. For a coefficient of friction of 0.2, the fault slips three times, and slip totals 5.48 m. On the other hand, a fault within a crust with a friction of 0.6 is not activated, while a fault in the reference model with a friction of 0.4 slips two times.

A 75° fault is only activated for a friction (μ_{back}) of 0.2 and slips more often than the 60° fault with at least 22 events (see Figure 5b). The fault shows larger offsets at the beginning, and after 12 events, it moves only 17 cm at each of the following events. The tectonic background stress is larger for a 75° fault (4.2 times the vertical stress S_V, Table 3) compared to a 60° fault (1.7 times S_V, Table 3). Therefore, larger fault offsets are related to the higher background stress and increased shear stresses.

For a coefficient of friction (μ_{back}) of 0.6, the 60° and 75° faults are not activated in our numerical simulations. The tectonic background stresses alone cannot reactivate these faults, and even the additional horizontal stresses due to GIA do not move these faults into an instability regime. The same is true for low-angle faults in a normal background regime, which are the opposite of steep-dipping faults in a thrusting regime as used in this study [e.g., *Abers*, 2009; *Bonini et al.*, 2012].

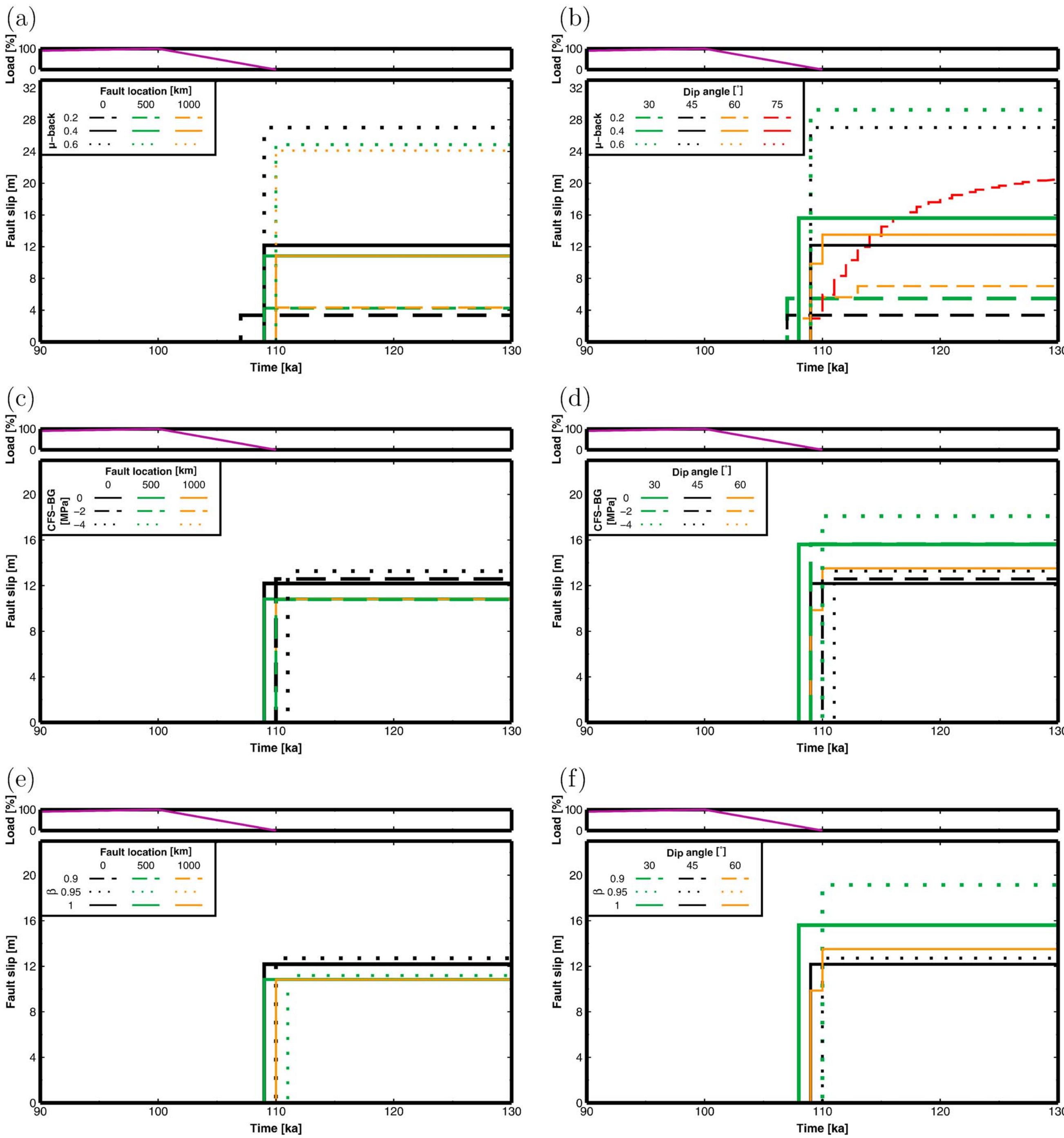

Figure 5. The effect of the following parameters on the activation time and magnitude of fault slip: (a and b) the coefficient of friction in the crust (μ_{back}), (c and d) CFS$^{\mathrm{BG}}$, and (e and f) β in addition to fault location (Figures 5a, 5c, and 5e) and fault angle (Figures 5b, 5d, and 5f). The time on the x axis refers to the model time running from 0 ka to 130 ka. No fault slip is obtained through the first 100 ka. The purple line in the upper diagram shows the distribution of the ice load during the model time. The following additional parameters were used: μ_{fault} of 0.4 and fault tip depth of 8 km.

In summary, fault throw and activation time are sensitive to the friction in the crust (μ_{back}), and large offsets of up to ~30 m can be produced by a coefficient of friction of 0.6. However, not all faults in a crust with this friction value are activated. On the other hand, steeply dipping faults with lower friction values do not reach a state of stability as evidenced by Figure 5b.

4.3. Influence of Change in Tectonic Background Stress (CFS^{BG} and β)

When the tectonic background stress falls below critical stress conditions, the activation of most faults is affected, and only faults below or close to the ice sheet center and with dips of 30° and 45° are activated (Figures 5c and 5d; see Table S2 in the supporting information).

A decrease in the tectonic background stress before glaciation leads to no fault activation for fault dips of 60° or more or if the faults are located at −1000 km or +1000 km away from the center of the model. If unstable conditions are obtained along the fault, a reduction in tectonic background stress causes the activation time to move from before to after the end of deglaciation. The later activation time correlates with an increase in fault slip as vertical stresses due to the load are smaller or no longer existent (see equations (4a) and (4b)). A CFS^{BG} of −2 MPa generates stress conditions such that a fault at ±500 km can be activated by GIA, but a further decrease to −4 MPa shows stable conditions for the whole glacial cycle. Thus, the crust along the weak zone in Laurentia and Fennoscandia cannot have initial fault stability much less than −2 MPa. In other words, to explain the localization of paleo and current intraplate earthquakes in Laurentia, we only need to assume that the initial fault stability is −4 MPa or more outside the earthquake zones.

A change in the parameter β from 1 to 0.95 shows that fault instability is not obtained for all faults tested in the model, and only 30° and 45° faults at the center or at ±500 km can be activated by GIA (Figure 5f). The activation time moves from before the end of deglaciation to a time point at or after it, which results in higher fault throws. For an even lower β of 0.9, no fault is activated. Therefore, lower values of β were not tested as stable conditions are predicted to prevail during the entire glacial cycle and afterward.

Assuming lower tectonic stress conditions at the beginning of the glacial cycle, some faults are not activated (e.g., 60°-dipping faults). Only below the ice sheet center, faults can be activated when the fault stability before glaciation was −4 MPa, which is accompanied by a decrease of horizontal stress of 4 MPa. Thus, the stress conditions before glaciation have to be close to the state of a critically stressed crust. Lower background stress conditions than for critical stress conditions show that most faults are not activated due to GIA. However, fault reactivation is observed in North America and Europe, implying that critical stress conditions are valid along the observed earthquake zones. Additionally, near-surface stress relief phenomena have been documented in formerly glaciated regions [*Pascal et al.*, 2010] indicating that the crust is critically stressed.

In summary, steeply dipping faults and faults located away from the ice sheet center are not activated if the crust is not critically stressed. Our models suggest that the horizontal background stresses were sufficiently low that without GIA no major earthquakes would have occurred along these faults. Earthquakes occur only when the crust is sufficiently close to a critical state that GIA can trigger fault reactivation, producing several meters of fault slip.

4.4. Influence of Friction of the Fault μ_{fault}

Fault slip magnitude increases with a decrease in coefficient of friction for the fault μ_{fault}. However, as tectonic background and GIA stresses are constant, the activation time is not changed (Figures 6a and 6b; see Table S3 in the supporting information).

The friction between opposing fault surfaces (μ_{fault}) gives an estimate of the resistance to displacement. Higher frictions lead to smaller movement, and therefore, smaller fault throws are obtained. This applies to all fault angles and locations. However, the difference in the slip between minimum and maximum friction decreases with a decreasing fault angle.

4.5. Influence of Depth of Fault Tip

The increase in the depth of the fault tip is accompanied by an increase in fault slip; however, the activation time of the fault remains constant, as tectonic background and GIA stresses are not changed by this parameter (Figures 6c and 6d; see Table S3 in the supporting information).

The fault slip magnitude is affected by the fault angle and depth of fault tip as the length of the fault is determined by these two parameters. A low-dipping fault is longer than a more steeply dipping fault with the tips at the same depths. The increase in fault slip due to deeper fault tips is induced by the length of the fault and also due to larger tectonic background stresses at deeper depths, since the stress increases with depth according to equation (3).

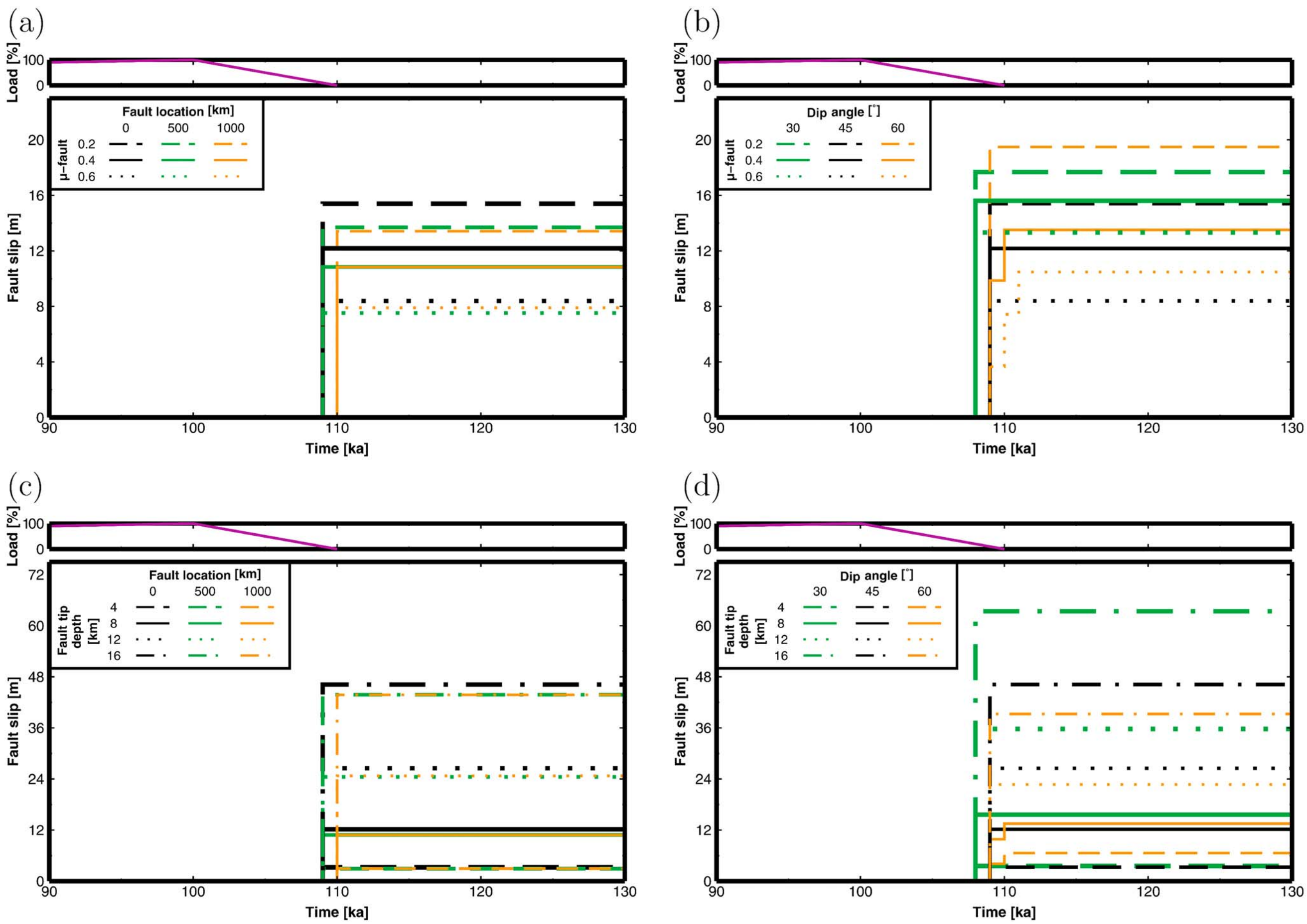

Figure 6. Similar to Figure 5, except for the coefficient of friction at the (a and b) fault (μ_{fault}) and (c and d) fault tip depth. The following additional parameters were used: μ_{back} of 0.4, CFS^{BG} of 0 MPa, and β of 1.

Faults at a location of +500 km show a lower fault throw for all depths of the fault tip than faults at −500 km. The difference between offsets on both sides of the center increases with an increase in fault tip depth. Faults at +1000 km and tips at 4 km and 8 km slip less than faults with the same tips at −1000 km. For larger depths of the fault tip, the behavior changes and faults at +1000 km slip up to 25 cm more than faults at −1000 km, but the activation time is constant. Faults on the positive side dip toward the ice sheet center, which induces higher stresses in the deeper parts of the faults. These stresses are higher compared to a fault at the same location on the other side of the ice sheet center (the negative side), as the fault tip is farther away from the ice sheet center due to the same dipping direction. The difference in the horizontal stress at fault tips on both sides of the model increases with an increase in the depth of the fault tip, and therefore, an increase in the difference of the fault throws is obtained or even a change in the maximum offset from the negative side to the positive side.

The activation time is the same for each fault and not sensitive to the depth of the fault tip. This is caused by a constant tectonic background stress and rebound stress applied to the model. However, the tectonic background stress increases with depth, and faults activated from deeper tips produce larger offsets as more stress is released, which controls the fault movement.

4.6. Relationship of Modeled Fault Slips to Earthquake Moment Magnitudes

In order to better appreciate the effects of GIA-induced fault slips along the GIF, we compute their earthquake moment magnitudes and compare them with some well-known large events triggered not by GIA. Moment magnitude (M_w) of earthquakes can be expressed in terms of displacement (D) along faults: $M_w = 2/3 \log(G \cdot D \cdot A) - 10.7$, where A is the surface area of the fault and G is the shear modulus of the

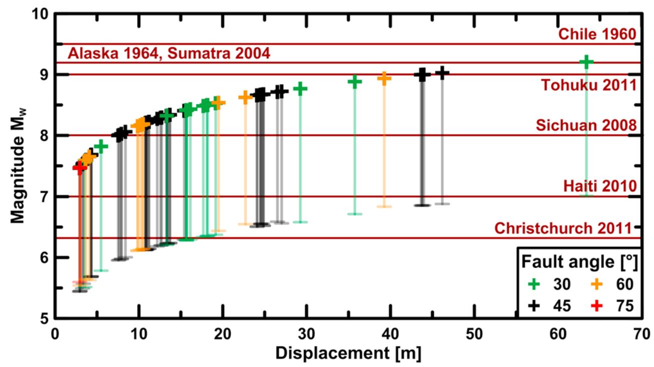

Figure 7. Moment magnitude of earthquakes due to the release of GIA stresses obtained within this study. The upper limit refers to values neglecting the surface rupture length, and the lower limit (end of vertical bar) is obtained using the length of the fault of 150 km, which is equivalent to the length of the Pärvie fault [*Juhlin et al.*, 2009]. The horizontal lines refer to major earthquakes during the last 100 years, which were not induced by GIA and without taking the displacement observed along these faults into account.

crust [*Hanks and Kanamori*, 1979]. However, the area A depends on the surface rupture length. As the length is not defined in a 2-D model, the longest mapped and best studied GIF is used as a reference value. The Pärvie fault in the Lapland Province in Sweden has a surface rupture length of 150 km [*Juhlin et al.*, 2009] and is therefore the longest observed and measured fault, which was activated due to the stress changes induced by GIA. However, there is another equation for the moment magnitude that depends on the displacement along the fault only and is independent of the fault length ($M_w = 6.853 + 1.306 \log D$ [*Hanks and Kanamori*, 1979; *Slemmons*, 1982; *Ekström and Dziewonski*, 1988]). The moment magnitudes obtained from the latter equation without inclusion of the surface rupture length is used as the maximum value, and the results estimated from the first equation using a surface rupture length of 150 km provides a reference value for a known GIF assuming that the entire fault was activated at the same time and there is no change in size during movement (Figure 7). To better appreciate their effect, the moment magnitudes of major earthquakes during the last 100 years are also plotted in Figure 7. These earthquakes are mostly related to subduction zones and are not induced by GIA. The physics between subduction zone earthquakes and GIF earthquakes is also different, and their moment magnitudes are only plotted for reference.

The moment magnitude obtained from a fault slip magnitude of 63 m and a fault length of 150 km falls within the range of 7.0 to 9.2 (Figure 7). These moment magnitudes are equivalent to earthquakes along subduction zones (e.g., Japan and Indonesia). As deglaciated regions are considered to be stable and typically consist of old cratons, earthquakes in this magnitude range are not generally expected. Observed GIFs in Fennoscandia suggest that events with magnitudes above 8.0 may have occurred at the end of the deglaciation [*Arvidsson*, 1996]. Observation and models thus indicate that GIA transformed a stable area into a tectonically active zone; however, models show that main activity terminates after only one or two earthquakes. Present-day observations show that seismicity still exists in formerly glaciated regions, but the magnitudes are mostly below 4.0 [e.g., *Lund et al.*, 2009; *Bungum et al.*, 2010; *Steffen and Wu*, 2011; *Steffen et al.*, 2012]. Present-day activity may actually be long-lived aftershock sequences [e.g., *Stein and Liu*, 2009].

5. Conclusions

In this study, the new 2-D finite element model of *Steffen et al.* [2014a] is used, which is based on the classic Anderson-Coulomb theory of fault stability. The physics of the model is simple and does not include dynamic processes such as Rice-Ruina stability, nucleation, or memory in slip. The advantage of this method is that it explicitly accounts for the role of GIA-induced stress changes in activating faults. Here the sensitivity of the magnitude of fault slip and activation time are tested with respect to the tectonic background stress and fault parameters.

Fault slips and activation times obtained within this study should be considered as preliminary values, as several simplifications have been made that impose limitations on their general applicability. For example, a simplified parabolic ice sheet is considered; consequently, effects of separate ice domes are neglected in our models. Furthermore, the lateral extent of the ice sheet is constant during loading and unloading phases. A simple stratified earth model is used, so the effects of lateral heterogeneity of material properties are not considered. The fault alone is also constrained in a number of respects: no cohesion is applied between opposing fault surfaces, the coefficient of friction is constant during a rupture, the fault tip is fixed, and the effects of pore fluid pressure are neglected. Nevertheless, our approach provides important new insights concerning GIF behavior in different stress settings and with respect to the dip angle of preexisting faults.

Faults are activated close to the end of deglaciation, and the slip magnitude depends mainly on the depth of the fault tip and, therefore, on the length of the fault. For consistency with prevailing stress regimes in Fennoscandia and Laurentia, the background stress regime is assumed to be of thrust/reverse type. The fault slips obtained within this study imply large-magnitude earthquakes (≥5.9), which are not expected in stable and old cratonic areas like eastern Canada and in the absence of GIA-induced stress perturbations.

Our modeling indicates that a fault with low dip angle slips only once, but steeply dipping faults may slip more. A limitation of our approach is that stress buildup at the fault tip is not accounted for. However, the slip magnitudes of subsequent events have smaller magnitudes compared to the main event. Observations and also results from our GIA-fault models show that transient stress perturbations due to GIA transformed a stable cratonic area into a tectonically active zone with earthquake magnitudes comparable to those found in subduction zones (e.g., Japan and Indonesia).

Below we summarize the answers to the questions raised in section 1:

1. The magnitude in tectonic background stress affects the activation time but only by a few thousand years after deglaciation.
2. The stress conditions before glaciation must be very close to a critically stressed crust; otherwise GIA is insufficient to trigger the observed intraplate earthquakes.
3. Steeply dipping faults can be activated if the coefficient of friction of the crust is assumed to be equal to or lower than 0.4.
4. Depth of fault tip and coefficient of friction along the fault affect the fault slip magnitude but do not influence the activation time as the GIA and tectonic background stress magnitudes are not changed.

The modeled fault slips fit well to observed data in North America and Europe. Major fault offsets observed in formerly glaciated regions are obtained within this study. However, many smaller offsets in the centimeter range exist [see *Fenton*, 1994] but are not produced by this model.

The answers of these questions have opened new problems, which need to be analyzed and tested to obtain a better understanding of fault slip magnitude and activation time due to GIA. For example, the effect of a changing pore fluid pressure was neglected within this study, but this factor has the potential to trigger GIFs. However, this parameter is insufficiently studied and will be the topic of a forthcoming paper. Moreover, cohesion along the fault plane was neglected, in part because preexisting faults generally have low cohesion. Nevertheless, this study has helped to answer several questions, and changes in fault slip magnitude and activation time could be related to these parameters: e.g., dip angle, coefficient of friction, fault stability before glaciation, and tectonic background stress factor. Future investigations will include the mentioned ideas above as well as the extension into a three-dimensional model.

Acknowledgments
We thank the Editors Onno Oncken and John Geissman and the reviewers Christophe Pascal and Erik Ivins for their constructive reviews and comments. We would like to thank Björn Lund (Uppsala University), Steffen Abe (RWTH Aachen), and Bernard Guest, Robert Taerum, and Len Hills (all from University of Calgary) for helpful discussions, for providing data sets, and for suggestions and comments on earlier versions of the manuscript. The research is supported by NSERC Discovery Grants to David W. Eaton and Patrick Wu. Figures 4–6 were drawn using the GMT graphics package [*Wessel and Smith*, 1998].

References

Abers, G. A. (2009), Slip on shallow-dipping normal faults, *Geology*, *37*, 767–768, doi:10.1130/focus082009.1.
Adams, J. (1989), Crustal stresses in eastern Canada, in *Earthquakes at North Atlantic Passive Margins: Neotectonics and Postglacial Rebound*, edited by S. Gregersen and P. W. Basham, pp. 289–297, Kluwer, Dordrecht, Netherlands.
Arvidsson, R. (1996), Fennoscandian earthquakes: Whole crustal rupturing related to postglacial rebound, *Science*, *274*, 744–746, doi:10.1126/science.274.5288.744.
Bonini, M., F. Sani, and B. Antonielli (2012), Basin inversion and contractional reactivation of inherited normal faults: A review based on previous and new experimental models, *Tectonophysics*, *522–523*, 55–88, doi:10.1016/j.tecto.2011.11.014.
Brandes, C., J. Winsemann, J. Roskosch, J. Meinsen, D. C. Tanner, S. Tsukamoto, M. Frechen, H. Steffen, and P. Wu (2012), Activity along the Osning thrust in central Europe during the late Weichselian: Ice-sheet and lithosphere interactions, *Quat. Sci. Rev.*, *38*, 49–62, doi:10.1016/j.quascirev.2012.01.021.
Bungum, H., O. Olesen, C. Pascal, S. Gibbons, C. Lindholm, and O Vestøl (2010), To what extent is the present seismicity of Norway driven by post-glacial rebound?, *J. Geol. Soc. London*, *167*, 373–384, doi:10.1144/0016-76492009-009.
Byerlee, J. D. (1978), Friction of rock, *Pure Appl. Geophys.*, *116*, 615–626, doi:10.1007/BF00876528.
Célérier, B. (1988), How much does slip on a reactivated fault plane constrain the stress tensor?, *Tectonics*, *7*, 1257–1278, doi:10.1029/TC007i006p01257.
Célérier, B. (1995), Tectonic regime and slip orientation of reactivated faults, *Geophys. J. Int.*, *121*, 143–161, doi:10.1111/j.1365-246X.1995.tb03517.x.
Dahl-Jensen, T., T. B. Larsen, and P. Voss (2010), Greenland ice sheet monitoring network (GLISN): A seismological approach, *Geol. Surv. Den. Greenl.*, *20*, 55–58.
Darbyshire, F., D. W. Eaton, and I. D. Bastow (2013), Seismic imaging of the lithosphere beneath Hudson Bay: Episodic growth of the Laurentian mantle keel, *Earth Planet. Sci. Lett.*, *373*, 179–193, doi:10.1016/j.epsl.2013.05.002.

Dyke, A. S., T. F. Morris, and D. E. C. Green (1991), Postglacial tectonic and sea level history of the central Canadian Arctic, *Bull. Geol. Surv. Can.*, *397*, 56.

Dziewonski, A. M., and D. L. Anderson (1981), Preliminary reference Earth model, *Phys. Earth planet. Inter.*, *25*, 297–356, doi:10.1016/0031-9201(81)90046-7.

Eaton, D. W., and F. Darbyshire (2010), Lithospheric architecture and tectonic evolution of the Hudson Bay region, *Tectonophysics*, *480*, 1–22, doi:10.1016/j.tecto.2009.09.006.

Eaton, D. W., F. Darbyshire, R. L. Evans, H. Grutter, A. G. Jones, and X. Yuan (2009), The elusive lithosphere-asthenosphere boundary (LAB) beneath cratons, *Lithos*, *109*, 1–22, doi:10.1016/j.lithos.2008.05.009.

Ekström, G., and A. M. Dziewonski (1988), Evidence of bias in estimations of earthquake size, *Nature*, *332*, 319–323, doi:10.1038/332319a0.

Fenton, C. (1994), Postglacial faulting in Eastern Canada, *Geol. Surv. Canada Open File Rep. 2774*, 94 pp., Natural Resources Canada.

Hampel, A., and R. Hetzel (2006), Response of normal faults to glacial-interglacial fluctuations of ice and water masses on Earth's surface, *J. Geophys. Res.*, *111*, B06406, doi:10.1029/2005JB004124.

Hanks, T. C., and H. Kanamori (1979), A moment magnitude scale, *J. Geophys. Res.*, *84*, 2358–2350, doi:10.1029/JB084iB05p02348.

Harris, R. A. (1998), Introduction to special section: Stress triggers, stress shadows, and implications for seismic hazard, *J. Geophys. Res.*, *103*, 24,347–24,358, doi:10.1029/98JB01576.

Hibbitt, D., B. Karlsson, and P. Sorensen (2012), *Getting Started With ABAQUS—Version (6.12)*, Hibbitt, Karlsson and Sorensen Inc, Pawtucket, R. I.

Hoffman, P. F. (1989), Precambrian geology and tectonic history of North America, in *The Geology of North America—An overview*, edited by A. W. Bally and A. R. Palmer, pp. 447–512, Geol. Soc. of Am., Boulder, Colo.

Ivins, E. R., T. H. Dixon, and M. P. Golombek (1990), Extensional reactivation of an abandoned thrust: A bound on shallowing in the brittle regime, *J. Struct. Geol.*, *12*, 303–314, doi:10.1016/0191-8141(90)90015-Q.

Ivins, E. R., T. S. James, and V. Klemann (2003), Glacial isostatic stress shadowing by the Antarctic ice sheet, *J. Geophys. Res.*, *108*(B12), 2560, doi:10.1029/2002JB002182.

Jakobsson, M., S. Björck, M. O'Regan, T. Flodén, S. L. Greenwood, H. Swärd, A. Lif, L. Ampel, H. Koyi, and A. Skelton (2014), Major earthquake at the Pleistocene-Holocene transition in Lake Vättern, southern Sweden, *Geology*, *42*, 379–382, doi:10.1130/G35499.1.

Johnston, A. C. (1987), Suppression of earthquakes by large continental ice sheets, *Nature*, *330*, 467–469, doi:10.1038/330467a0.

Johnston, P., P. Wu, and K. Lambeck (1998), Dependence of horizontal stress magnitude on load dimension in glacial rebound models, *Geophys. J. Int.*, *132*, 41–60, doi:10.1046/j.1365-246x.1998.00387.x.

Juhlin, C., M. Dehghannejad, B. Lund, A. Malehmir, and G. Pratt (2009), Reflection seismic imaging of the end-glacial Pärvie Fault system, northern Sweden, *J. Appl. Geophys.*, *70*, 307–316, doi:10.1016/j.jappgeo.2009.06.004.

Kim, Y.-S., and D. J. Sanderson (2005), The relationship between displacement and length of faults: A review, *Earth Sci. Rev.*, *68*, 317–334, doi:10.1016/j.earscirev.2004.06.003.

Kinck, J. J., E. S. Husbye, and F. R. Larsson (1993), The Moho depth distribution in Fennoscandia and the regional tectonic evolution from Archean to Permian times, *Precambrian Res.*, *64*, 23–51, doi:10.1016/0301-9268(93)90067-C.

Kujansuu, R. (1964), Nuorista siirroksista Lappissa. Summary: Recent faults in Lapland, *Geologi*, *16*, 30–36.

Kukkonen, I. T., K. A. Kinnunen, and P. Peltonen (2003), Mantle xenoliths and thick lithosphere in the Fennoscandian shield, *Phys. Chem. Earth*, *28*, 349–360, doi:10.1016/S1474-7065(03)00057-3.

Lagerbäck, R. (1978), Neotectonic structures in northern Sweden, *Geol. Foeren. Stockholm Foerh.*, *100*, 263–269, doi:10.1080/11035897809452533.

Lagerbäck, R., and M. Sundh (2008), *Early Holocene Faulting and Paleoseismicity in Northern Sweden*, 836, Sveriges geologiska undersökning—Research paper, Uppsala, Sweden.

Larsen, T. B., T. Dahl-Jensen, P. Voss, T. M. Jørgensen, S. Gregersen, and H. P. Rasmussen (2006), Earthquake seismology in Greenland—Improved data with multiple applications, *Geol. Surv. Den. Greenl.*, *10*, 57–60.

Lund, B. (2005), Effects of deglaciation on the crustal stress field and implications for endglacial faulting: A parametric study of simple Earth and ice models, *Tech. Rep. TR-05-04*, Swedish Nucl. Fuel. Waste Manage. Co., Stockholm, Sweden.

Lund, B., and M. D. Zoback (1999), Orientation and magnitude of in situ stress to 6.5 km depth in the Baltic Shield, *Int. J. Rock Mech. Min. Sci.*, *36*, 169–190, doi:10.1016/S0148-9062(98)00183-1.

Lund, B., P. Schmidt, and C. Hieronymus (2009), Stress evolution and fault stability during the Weichselian glacial cycle, *Tech. Rep. TR-09-15*, Swedish Nucl. Fuel. Waste Manage. Co., Stockholm, Sweden.

Luttrell, K., and D. Sandwell (2010), Ocean loading effects on stress at near shore plate boundary fault systems, *J. Geophys. Res.*, *115*, B08411, doi:10.1029/2009JB006541.

Mazotti, S., and J. Townend (2010), State of stress in central and eastern North American seismic zones, *Lithosphere*, *2*, 76–83, doi:10.1130/L65.1.

Muir-Wood, R. (1993), A review of the seismotectonics of Sweden, *Tech. Rep. TR-93-13*, Swedish Nucl. Fuel Waste Manage. Co., Stockholm, Sweden.

Munier, R., and C. Fenton (2004), Review of postglacial faulting—Current understanding and directions for future studies, in *Respect Distances—Rationale and Means of Computation, Rep. R-04-17*, 62 pp., Swedish Nucl. Fuel. Waste Manage. Co., Stockholm, Sweden.

Nüchter, J.-A., and S. Ellis (2010), Complex states of stress during the normal faulting seismic cycle: Role of midcrustal postseismic creep, *J. Geophys. Res.*, *115*, B12411, doi:10.1029/2010JB007557.

Olesen, O. (1988), The Stuoragurra Fault, evidence of neotectonics in the Precambrian of Finnmark, northern Norway, *Nor. Geol. Tidsskr.*, *68*, 107–118.

Pascal, C., D. Roberts, and R. H. Gabrielsen (2010), Tectonic significance of present-day stress relief phenomena in formerly glaciated regions, *J. Geol. Soc. London*, *167*, 363–371, doi:10.1144/0016-76492009-136.

Quinlan, G. (1984), Postglacial rebound and the focal mechanisms of eastern Canadian earthquakes, *Can. J. Earth Sci.*, *21*, 1018–1023, doi:10.1139/e84-106.

Rivera, L., and H. Kanamori (2002), Spatial heterogeneity of tectonic stress and friction in the crust, *Geophys. Res. Lett.*, *29*, 1088, doi:10.1029/2001GL013803.

Sauber, J., and B. Molnia (2004), Glacier ice mass fluctuations and fault instability in tectonically active southern Alaska, *Global Planet. Change*, *42*, 279–293, doi:10.1016/j.gloplacha.2003.11.012.

Shilts, W. W., M. Rappol, and A. Blais (1992), Evidence of late and postglacial seismic activity in the Témiscouata–Madawaska Valley, Quebec–New Brunswick, Canada, *Can. J. Earth Sci.*, *29*, 1043–1059, doi:10.1139/e92-085.

Slemmons, D. B. (1982), Determination of design earthquake magnitudes for microzonation, in *Proceedings of the 3rd International Earthquake Microzination Conference*, vol. 1, pp. 119–130, Seattle, Wash.

Slunga, R. (1991), The Baltic shield earthquakes, *Tectonophysics*, *189*, 323–331, doi:10.1016/0040-1951(91)90505-M.

Smith, C. A., M. Sundh, and H. Mikko (2014), Surficial geology indicates early Holocene faulting and seismicity, central Sweden, *Int. J. Earth Sci.*, doi:10.1007/s00531-014-1025-6.

Steffen, H., and G. Kaufmann (2005), Glacial isostatic adjustment of Scandinavia and northwestern Europe and the radial viscosity structure of the Earth's mantle, *Geophys. J. Int.*, *163*, 801–812, doi:10.1111/j.1365-246X.2005.02740.x.

Steffen, H., and P. Wu (2011), Glacial isostatic adjustment in Fennoscandia—A review of data and modeling, *J. Geodyn.*, *52*, 169–204, doi:10.1016/j.jog.2011.03.002.

Steffen, H., J. Müller, and H. Denker (2009), Analysis of mass variations in northern glacial rebound areas from GRACE data, in *Observing Our Changing Earth, IAG Symposia Ser.,* vol. 133, edited by M. G. Sideris, pp. 501–509, Springer, Berlin Heidelberg, doi:10.1007/978-3-540-85426-5_60.

Steffen, H., G. Kaufmann, and R. Lampe (2014c), Lithosphere and upper-mantle structure of the southern Baltic Sea estimated from modelling relative sea-level data with glacial isostatic adjustment, *Solid Earth*, *5*, 447–459, doi:10.5194/se-5-447-2014.

Steffen, R., D. W. Eaton, and P. Wu (2012), Moment tensors, state of stress and their relation to post-glacial rebound in northeastern Canada, *Geophys. J. Int.*, *189*, 1741–1752, doi:10.1111/j.1365-246X.2012.05452.x.

Steffen, R., P. Wu, H. Steffen, and D. W. Eaton (2014a), On the implementation of faults in finite-element glacial isostatic adjustment models, *Comput. Geosci.*, *62*, 150–159, doi:10.1016/j.cageo.2013.06.012.

Steffen, R., P. Wu, H. Steffen, and D. W. Eaton (2014b), The effect of earth rheology and ice-sheet size on fault-slip and magnitude of postglacial earthquakes, *Earth Planet. Sci. Lett.*, *388*, 71–80, doi:10.1016/j.epsl.2013.11.058.

Stein, S., N. Sleep, R. Geller, S. Wang, and G. Kroeger (1979), Earthquakes along the passive margin of eastern Canada, *Geophys. Res. Lett.*, *5*, 537–540, doi:10.1029/GL006i007p00537.

Stein, S., S. Cloetingh, N. Sleep, and R. Wortel (1989), Passive margin earthquakes, stresses, and rheology, in *Earthquakes at North Atlantic Passive Margins: Neotectonics and Postglacial Rebound*, edited by S. Gregersen and P. W. Basham, pp. 231–259, Kluwer, Dordrecht.

Stein, S., and M. Liu (2009), Long aftershock sequences within continents and implications for earthquake hazard assessment, *Nature*, *462*, 87–89, doi:10.1038/nature08502.

Suppe, J. (1985), *Principles of Structural Geology*, pp. 537, Prentice-Hall, New Jersey.

Turpeinen, H., A. Hampel, T. Karow, and G. Maniatis (2008), Effect of ice growth and melting on the slip evolution of thrust faults, *Earth Planet. Sci. Lett.*, *269*, 230–241, doi:10.1016/j.epsl.2008.02.017.

Twiss, R. J., and E. M. Moores (2007), *Structural Geology*, 2nd ed., W. H. Freeman, New York.

Voss, P., S. K. Poulsen, S. B. Simonsen, and S. Gregersen (2007), Seismic hazard assessment of Greenland, *Geol. Surv. Den. Greenl.*, *13*, 57–60.

Watts, A. B., and E. B. Burov (2003), Lithospheric strength and its relationship to the elastic and seismogenic layer thickness, *Earth Planet. Sci. Lett.*, *213*, 113–131, doi:10.1016/S0012-821X(03)00289-9.

Wessel, P., and W. H. F. Smith (1998), New, improved version of generic mapping tools released, *Eos Trans. AGU*, *79*, 579.

Wu, P. (1996), Changes in orientation of near-surface stress field as constraints to mantle viscosity and horizontal stress differences in eastern Canada, *Geophys. Res. Lett.*, *23*, 2263–2266, doi:10.1029/96GL02149.

Wu, P. (1997), Effect of viscosity structure on fault potential and stress orientations in eastern Canada, *Geophys. J. Int.*, *130*, 365–382, doi:10.1111/j.1365-246X.1997.tb05653.x.

Wu, P. (2004), Using commercial finite element packages for the study of earth deformations, sea levels and the state of stress, *Geophys. J. Int.*, *158*, 401–408, doi:10.1111/j.1365-246X.2004.02338.x.

Wu, P., and H. S. Hasegawa (1996a), Induced stresses and fault potential in Eastern Canada due to a disc load: A preliminary analysis, *Geophys. J. Int.*, *125*, 415–430, doi:10.1111/j.1365-246X.1996.tb00008.x.

Wu, P., and H. S. Hasegawa (1996b), Induced stresses and fault potential in eastern Canada due to a realistic load: A preliminary analysis, *Geophys. J. Int.*, *127*, 215–229, doi:10.1111/j.1365-246X.1996.tb01546.x.

Zoback, M. L. (1992), Stress field constraints on intraplate seismicity in eastern north America, *J. Geophys. Res.*, *97*, 11,761–11,782, doi:10.1029/92JB00221.

